Prediction of solid state structure based on eutectic and eutectoid transformation parameters in spheroidal graphite irons

J. Sertucha[1], R. Suárez*[1], J. Izaga[1], L. A. Hurtado[2] and J. Legazpi[2]

The aim of the present work is to predict experimentally the structural trend of liquid iron based on its solidification features and the subsequent solid state transition. Both transformation processes in SG iron samples are simultaneously studied by means of industrial thermal analysis techniques. Experimental parameters are established in both cases in order to quantify the main metallurgical facts and correlate them with the structural properties of different alloys used in real manufacturing processes. A computer aided program has been designed for the treatment of the cooling curves.

A large number of experimental tests using different chemical compositions were made. After curves treatment, several studies have been conducted to correlate the thermal parameters obtained and the structural properties detected via metallographic inspections. The influence of the solidification parameters on carbon diffusion process and the resulting structures is discussed. A new structural model was developed in order to predict the ferrite content on the basis of thermal evolution of SG iron. Nucleation potential (inoculation grade), carbide formation tendency and solid state evolution of metal are evaluated and final structure distribution is accurately estimated.

Keywords: Solid state, Structure, Eutectic transformation, Eutectoid transformation, Spheroidal iron

Introduction

In the last decades, thermal analysis techniques have been used in foundries as an experimental method to obtain information about the chemical composition (carbon equivalent) of irons,[1,2] inoculation efficiency, mechanical properties,[3] graphite shape,[4] latent heat calculations,[4–7] graphitic nucleation potential during the solidification,[8] shrinkage tendency in cast alloys,[9] oxidation state of the iron[10] and hardness prediction.[11] Based on these analyses, several systems relating cooling curves to casting properties have been developed and applied in foundry processes. However, such results are not interchangeable among foundries and an important effort is necessary in order to know their specific metallurgical characteristics.

The main thrust of previous work on the application of thermal analysis for foundry use was directed to the eutectic (liquid–solid) transformation. In the present work, both eutectic and eutectoid (solid–solid transition) are considered for a whole treatment of solidification and cooling. In graphitic irons, the eutectoid transformation represents the ferrite and/or pearlite formation and, therefore, provides the mechanical properties of material at room temperature. An example of cooling curves obtained in the present work is shown in Fig. 1.

The prediction of mechanical properties in ductile iron castings is connected to the knowledge of the liquid–solid and solid–solid transformation phenomena.[12] The information analysed from the cooling curves recorded in the eutectoid area is as important as the one obtained in the solidification range. In the last case graphite nucleation potential is defined, while chemical composition and cooling rate parameters are included in solid state transition.

In a previous work, Guo and Stefanescu[13] have studied the effect of different cooling rates in the eutectoid range and the final structure of ferritic and pearlitic composition samples. In the present work, the normal solidification and cooling processes of different nodular irons (modifying only the Cu and Mn contents) are investigated under industrial conditions, using similar cooling rates ($\sim$50 K min^{-1}) for inoculated and non-inoculated standard samples.

After recording the thermal curves and examining the final structure of both samples, the authors have compared them and established a final relationship which will be discussed in following sections. The present paper is a partial report based on the thermal analysis work conducted at Betsaide, S.A.L. foundry. It

[1]Azterlan Foundry Centre, E-48200 Durango (Bizkaia), Spain
[2]Betsaide, S.A.L. Foundry, E-48230 Elorrio (Bizkaia), Spain

*Corresponding author, email rsuarez@azterlan.es

© 2006 W. S. Maney & Son Ltd.
DOI 10.1179/136404606X167114

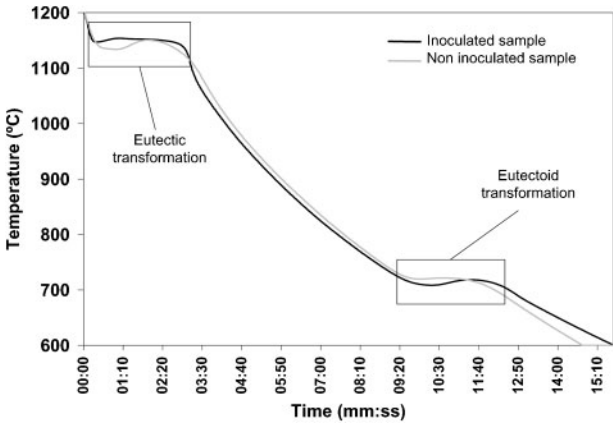

1 Cooling curves for inoculated and non-inoculated nodular iron samples

is related to the prediction of the final structure in cast parts before pouring operations.

Experimental

An extensive number of solidification experiments were performed on ductile iron qualities from EN GJS 400-15U to EN GJS 700-2U. The cast samples were obtained from the three 230 Disamatic moulding lines equipped with automatic pouring furnaces (7 t of capacity and references ABB-CTO5 and ABB-OCC50 installed at Betsaide, S.A.L.). Poured moulds are cooled into a 50–55 m line before final shaking out. The measured samples were picked from the pouring furnaces in the basin area close to the rod stopper (Fig. 2).

The experiments were carried out using a Thermolan thermal analysis system (Fig. 3) developed in Azterlan Foundry Centre. All the cooling curves were recorded, their critical parameters were determined and the results were obtained through a computer aided program adapted for this purpose.

The liquid metal samples used in the present work were melted in three medium frequency induction furnaces (250 Hz), 10 t in capacity and 5000 kW in power. The metallic charge is composed of 40% automotive steel scrap, 10% pig iron and 50% return scrap. After melting, carbon and silicon contents were checked and adjusted to the specified values. The liquid metal temperature was then increased up to 1500°C and its surface skimmed.

After final conditioning, the melt was treated in a 2 t capacity ladle with a noduliser alloy (FeSiMg 522) by means of the tundish cover method. The treatment temperatures were in the range of 1480–1500°C. When

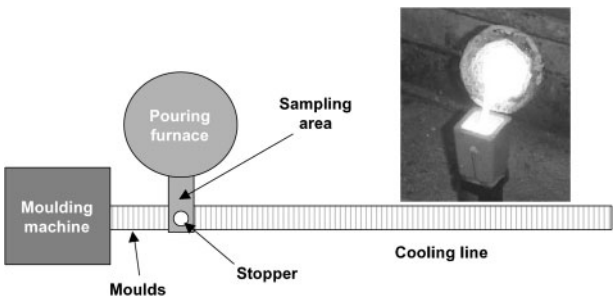

2 Scheme of moulding line and sampling method

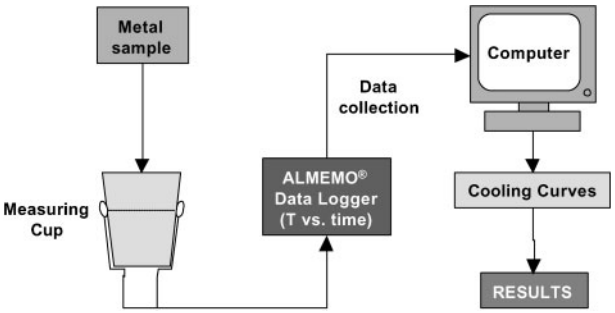

3 Scheme of thermal analysis system used in experimental measurements

the reaction was accomplished, the treated batch was transferred to the corresponding pouring furnace.

In all cases, the samples were poured into commercial cups (Quik-Cup with a type k thermocouple located at the centre of the cup) without tellurium. Simultaneously, two cups (inoculated and non-inoculated) were cast and analysed in each thermal test. Approximately 0·15% of commercial inoculant product (Si=74·5%, Ca=2·41%, Zr=1·50% and Al=1·21%) was introduced in one of the cups before pouring. In addition, special samples were collected for later chemical analysis (the results are presented in Table 1).

So as to cover a wide ferrite/pearlite ratio, six different chemical compositions based on silicon, manganese and copper contents were selected. Three tests were made on different days for each quality with the aim of comparing the reproducibility of the results obtained and optimising their reliability.

The temperature range recorded in the thermal analysis was 1210–600°C in order to study both solidification and solid state transitions (Fig. 1) in all samples. The accurate way of the measuring process requires a sampling cup with a very high consistency. The following conditions are needed for correct analysis:

(i) as the maximum capacity of the pouring cups is 310–320 g, a minimum weight may be needed to obtain representative results

Table 1 Results of chemical characterisation of ductile iron samples

	Element content, %				
Sample	Carbon	Silicon	Manganese	Copper	Magnesium
1-1	3·77	2·57	0·11	0·05	0·032
1-2	3·76	2·60	0·12	0·08	0·032
1-3	3·53	2·41	0·15	0·06	0·030
2-1	3·65	2·71	0·14	0·15	0·037
2-2	3·64	2·69	0·14	0·13	0·033
2-3	3·67	2·66	0·14	0·16	0·033
3-1	3·79	2·67	0·12	0·27	0·036
3-2	3·80	2·64	0·12	0·27	0·033
3-3	3·66	2·52	0·15	0·33	0·026
4-1	3·77	2·84	0·12	0·40	0·032
4-2	3·72	2·71	0·13	0·42	0·034
4-3	3·76	2·53	0·13	0·32	0·033
5-1	3·70	2·60	0·12	0·75	0·036
5-2	3·88	2·54	0·09	0·74	0·035
5-3	3·71	2·76	0·12	0·73	0·037
6-1	3·60	2·60	0·12	0·90	0·030
6-2	3·64	2·60	0·13	0·90	0·032
6-3	3·66	2·54	0·15	0·92	0·042

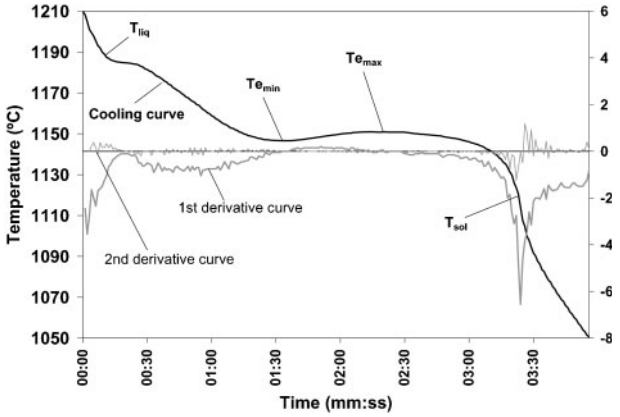

4 Critical parameters in liquid–solid transformations

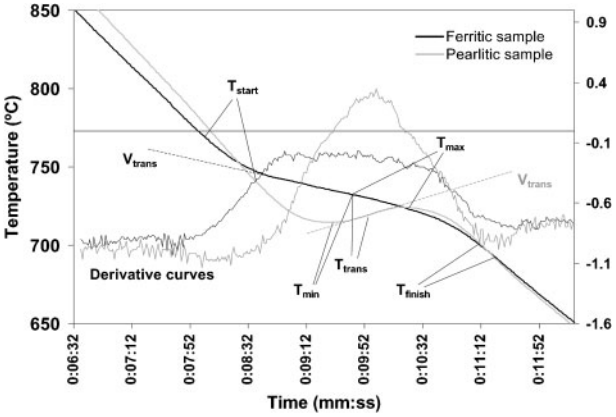

5 Critical parameters in solid state transformations

(ii) the sand from the sampling cups should not be coated and react with the melt
(iii) the weight of samples should be constant
(iv) stable conditions at the sampling cups are needed during the process of data collection.

After thermal experiments, the metal samples contained in cups were cut and prepared for metallographic inspection. Optical microscopy observations were carried out in the central areas of the samples (where k type thermocouples are located in the measuring cups).

Nodule count was estimated following an experimental method developed by Azterlan Foundry Centre and included into the thermal analysis system used for data treatment. This estimation method comes from a previous study including the cooling curve parameters and metallographic nodule counts obtained by comparing the unetched sample structure with a set of microphotographs used as standard nodule count references.

After estimation of nodule counts using thermal parameters, all metallographic samples were etched in 5% nital ethanolic solution and the percentages of structural phases were estimated by a comparison with the standard references published by AFS.[14,15]

Results

Two groups of 18 and 36 metal samples (mainly ferritic, pearlitic and mixed structural grades, based on copper content) were chemically and thermally analysed respectively. The chemical compositions of the samples are presented in Table 1.

Thermal analysis tests were performed in the range of 1210–600°C in all cases. Eutectic phase transformations occur ~1130–1150°C, while eutectoid transitions are detected <770°C. Carbon and silicon contents of cast iron mainly affect the T_{liquidus} evolution. Inoculated samples show similar curve shapes, while non-inoculated ones provide an extensive variety of solidification patterns.

All thermal curves obtained were analysed, and their critical parameters were determined using the first and second derivative curves. Figures 4 and 5 show the selected points in each phase transition. In the eutectic cases, four transition temperatures (T_{liquidus}, Te_{min}, Te_{max} and T_{solidus}) and the recalescence parameter (Te_{max}–Te_{min}) were defined. Additional nodule count estimation values are obtained by analysing the curve shape and the graphite austenite growth pattern during the solidification processes.[16]

The evolution of the eutectic parameters is strongly modified by the inoculation (Table 2). As expected, liquid–solid transition temperatures increase and recalescences decrease when the nucleation potential of the metal becomes larger.

The solid–solid structural transitions (Fig. 5) are characterised by five temperature values (T_{start}, T_{min}, T_{trans}, T_{max} and T_{finish}), the corresponding recalescence (T_{max}–T_{min}) and the transition cooling rate V_{trans} measured at the point of inflection of the eutectoid transformation. T_{trans} corresponds to this point and it is calculated using the maximum of the first derivative curve.

Inoculated curves indicate similar nodularity and nodule count, without being conditioned by the original quality of liquid iron. The opposite fact is clearly revealed in non-inoculated samples, where nodule shape and nodule count depend highly on the nucleation potential of the treated metal before inoculation. The computer estimation of nodule count represents this behaviour accurately (Table 2). The solid state transformations provide cooling curves whose shape and temperature ranges show a clear dependence on the chemical composition of the inoculated samples (Table 3). Transition temperatures T_{trans} increase and recalescences decrease when the copper contents are low and the silicon content is high. This general behaviour is obtained by comparing very similar geometric moduli and, therefore, cooling rates.

Microstructural observations on inoculated samples show the expected ferrite and pearlite evolution according to the chemical composition of the cast iron (Cu, Si and Mn). Thus, an experimental relationship seems to exist between the eutectoid cooling curves and the metallic structures obtained by metallographic analysis.

In non-inoculated cases, more extensive structural results are obtained owing to the different nucleation potentials detected in the corresponding eutectic zones (Table 3). Cementite (Fe_3C) was observed in two non-inoculated samples (1-3 and 3-3). These phenomena can be easily detected by analysing the Te_{min} value from the eutectic transformation (Table 2).

Discussion

The prediction of casting technical properties is the ultimate aim of thermal analysis. However, this is a very

difficult task because there are many different chemical compositions in used alloys, section sizes, manufacturing conditions and consequently different solidification and cooling patterns in real castings.

Although all these factors must be considered in order to explain the final metallic structure of specific castings, the present work analyses the structural tendency of poured metal, based on its solidification and subsequent cooling processes. Therefore, the standard conditions used for thermal experiments (sample size and cooling rate) and the obtained results have also been used to predict the structure at room temperature in inoculated and non-inoculated samples. This fact represents an important development in order to design preventive control tools before the pouring operation, as an alternative method to metallographic analysis in cast iron production lines.

Based on previous work and the experimental results discussed above, the information analysed from the cooling curves at the liquid–solid transition is as important as the one obtained in the solid state range. All results obtained in the present work indicate that the final structure in castings is a consequence of several aspects related to the solidification and the following eutectoid transformation.

Usually the ferrite and pearlite formation is mainly related to the chemical composition and the cooling rate (size) of the analysed casting section. These two parameters affect the graphite growth process in solid state and define the eutectoid transition characteristics.

However, the nucleation potential of the iron is also an extremely critical parameter. After nucleation at primary austenite grains (eutectic area), the carbon atoms diffuse through the austenite shells that envelop the graphitic nodules. These phenomena affect the subsequent solid state transformation of austenite to ferrite and/or pearlite. Thus, in high nodule count samples (the inoculated ones for example) the carbon diffusion process in austenite is favoured by the high number of graphite austenite contact surfaces and ferrite formation is more likely to occur in similar chemical compositions and cooling rates.

Figure 6 shows the inoculating effect in all the standard samples analysed in the present work. In all cases, the inoculant additions increase the nucleation potential of the liquid alloy and the resulting nodule count in the solid state. Therefore, higher ferrite amounts are obtained in subsequent metallographic inspections.

The inoculation process provides nodule count estimations into the range of 225–325 nodules mm^{-2} in all the analysed samples. The metallographic inspections carried out confirm these graphite estimations. The variability of the non-inoculated samples (from 7 to 225

Table 2 Thermal parameters obtained from eutectic transformations

		Eutectic thermal parameters, °C				
Sample	Inoculation	$T_{liquidus}$	Te_{min}	Recalescence	$T_{solidus}$	Nodules mm^{-2} estimation
1-1	yes	1159·8	1153·4	2·0	1101·6	289
	no	1139·9	1128·4	20·9	1076·6	31
1-2	yes	1164·3	1152·6	0·9	1107·9	313
	no	1146·0	1137·7	5·7	1089·2	170
1-3	yes	1155·4	1147·4	3·0	1114·0	287
	no	1154·7	1118·2	7·9	1096·0	7
2-1	yes	1154·9	1153·3	4·4	1112·7	273
	no	1148·7	1137·0	9·1	1086·6	141
2-2	yes	1158·8	1151·8	5·3	1115·5	315
	no	1144·2	1136·5	8·3	1086·0	147
2-3	yes	1158·7	1153·8	3·9	1109·2	306
	no	1142·9	1135·2	9·1	1088·6	128
3-1	yes	1159·6	1154·6	2·2	1102·0	298
	no	1151·6	1138·1	0·2	1084·3	179
3-2	yes	1189·5	1154·6	2·2	1109·5	291
	no	1151·8	1138·0	3·0	1082·5	158
3-3	yes	1154·9	1145·2	5·5	1105·1	273
	no	1144·3	1112·7	2·9	1081·0	51
4-1	yes	1159·9	1155·8	2·1	1108·7	313
	no	1148·4	1145·6	2·2	1080·4	185
4-2	yes	1158·2	1155·6	2·3	1108·6	307
	no	1147·4	1145·4	1·5	1088·8	218
4-3	yes	1161·4	1153·3	1·3	1097·2	307
	no	1157·6	1144·2	4·1	1079·2	186
5-1	yes	1161·2	1154·2	1·6	1103·5	308
	no	1145·1	1135·0	11·6	1093·3	110
5-2	yes	1153·0	1145·5	7·1	1112·3	273
	no	1143·0	1125·5	15·8	1174·0	37
5-3	yes	1173·6	1155·4	2·3	1109·8	310
	no	1148·6	1146·1	1·3	1086·8	225
6-1	yes	1156·8	1151·3	5·4	1113·0	297
	no	1146·8	1128·5	24·4	1092·5	25
6-2	yes	1157·1	1149·7	6·1	1104·6	277
	no	1145·7	1139·1	11·6	1085·9	143
6-3	yes	1150·2	1143·4	6·3	1104·8	228
	no	1139·4	1137·8	1·0	1079·2	188

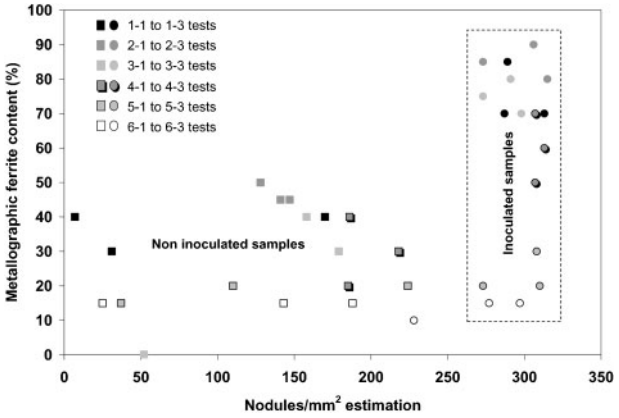

6 Ferrite evolution in inoculated and non-inoculated samples analysed in present work

nodules mm^{-2}) is a consequence of the different metallurgical qualities of liquid iron when samples were taken from the basin of the pouring furnace.

Taking into account similar chemical compositions in samples, distinguished by colours in Fig. 6, inoculation (higher nodule counts) increases the ferrite content in the final solid state structure (Fig. 7*a* and *b*). This behaviour is gradually minimised in copper alloyed samples (pearlitic grades). This kind of pearlite promoting elements prevents the carbon diffusion in austenite during solidification and cooling processes, and structural pearlite formation takes place.

Prevention of carbon diffusion in solid austenite provides chemical reactions between this element and the crystallised iron atoms. Small sheets of cementite are consequently formed and pearlite occurs during the solid state transformation. The standard samples used in the present work have very similar cooling rates, therefore, the structural tendency of cast iron was studied on the basis of its metallurgical characteristics (cooling curves type) and the chemical composition.

Taking into account the eutectic transformation, another structural component must be considered. Cementite (Fe_3C) can be formed as a consequence of low nucleation potentials in the iron and/or high cooling rates. Thus, graphite crystallisation is not favoured and iron carbides occur. Both thermal curves (solidification and solid state) can easily detect these phenomena. The primary cementite formation decreases the amount of austenite crystallised during solidification and therefore, reduces the energy involved in eutectoid transformation (Fig. 8).

The results obtained from thermal experiments carried out in the present work indicate that the graphite nucleation, subsequent nodules growth and the solid

Table 3 Thermal parameters obtained from solid state (eutectoid) transformations

		Eutectoid thermal parameters						
Sample	Inoculation	T_{start}, °C	T_{min}, °C	Recalescence	T_{trans}, °C	T_{finish}, °C	V_{trans}, K s^{-1}	Ferrite, %*
1-1	yes	753·9	739·3	0·0	739·3	710·7	−0·164	85
	no	758·6	732·2	0·0	732·2	718·9	−0·055	30
1-2	yes	749·8	729·3	0·1	729·4	711·8	−0·097	70
	no	755·1	727·0	0·4	727·1	716·2	0·027	40
1-3	yes	750·8	729·8	0·0	729·8	710·2	−0·118	70
	no	765·3	751·5	0·0	751·5	724·7	−0·236	40†
2-1	yes	762·1	748·1	0·0	748·1	711·9	−0·127	85
	no	760·4	724·4	0·0	724·4	717·2	−0·073	45
2-2	yes	758·7	744·4	0·0	744·4	711·7	−0·100	80
	no	757·6	722·1	0·0	722·1	714·3	−0·027	45
2-3	yes	759·2	747·3	0·0	747·3	706·3	−0·082	85
	no	758·5	724·7	0·0	724·7	702·1	−0·055	50
3-1	yes	750·9	733·7	0·0	733·7	715·7	−0·118	70
	no	752·9	730·9	0·2	730·9	718·1	0·018	30
3-2	yes	754·5	737·9	0·0	737·9	713·6	−0·118	80
	no	756·4	731·2	0·4	730·4	715·7	0·027	40
3-3	yes	746·0	728·5	0·0	728·5	709·5	−0·109	75
	no	784·2	781·4	0·0	781·4	695·0	−0·345	0†
4-1	yes	744·9	725·2	0·5	725·4	717·4	0·045	60
	no	755·2	725·5	0·2	725·5	717·6	0·027	20
4-2	yes	734·0	722·5	4·3	724·6	718·7	0·173	45
	no	738·3	721·8	4·0	723·7	717·0	0·191	30
4-3	yes	739·8	726·0	0·0	726·0	711·4	−0·018	70
	no	738·7	722·0	3·4	723·2	714·3	0·118	40
5-1	yes	725·1	716·0	5·6	719·5	714·4	0·191	30
	no	731·4	723·1	2·2	724·4	714·4	0·082	20
5-2	yes	734·6	719·1	2·3	720·4	710·7	0·082	15
	no	746·5	730·4	0·0	730·4	701·6	−0·045	15
5-3	yes	741·5	722·2	9·5	719·7	716·1	0·291	20
	no	723·1	716·4	5·8	719·6	711·2	0·164	20
6-1	yes	720·7	711·2	7·9	715·4	707·5	0·200	15
	no	734·3	719·8	1·0	720·1	696·5	0·045	15
6-2	yes	719·6	710·7	10·1	717·2	708·4	0·255	15
	no	719·9	713·1	5·4	715·9	709·1	0·218	10
6-3	yes	713·8	706·1	11·0	712·0	707·2	0·264	10
	no	717·2	706·7	11·0	711·0	696·4	0·245	15

*Pearlite contents correspond to 100 minus ferrite per cent.
†Cementite (Fe_3C) was detected in metallographic inspections, especially in test 3-3.

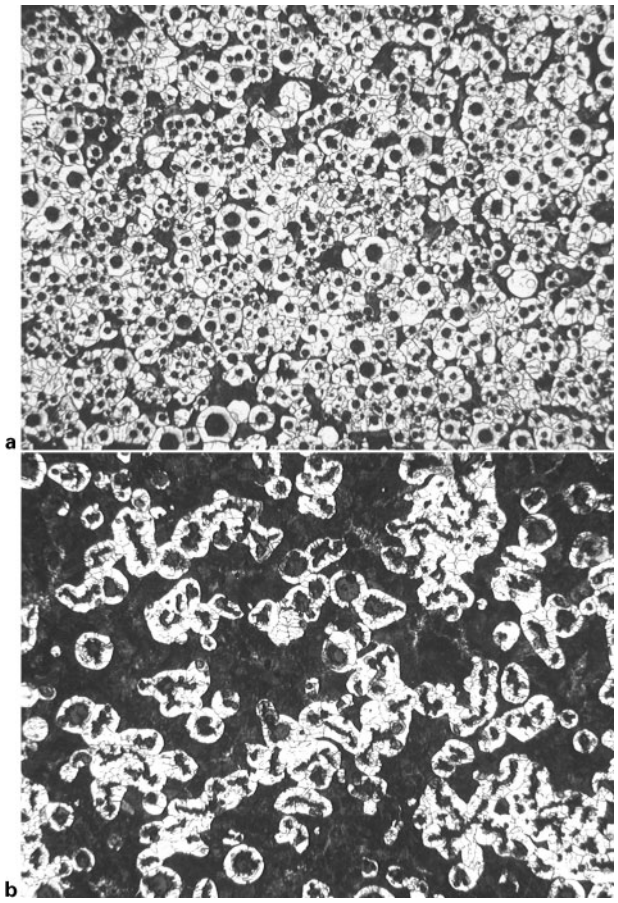

7 Microstructures of *a* inoculated and *b* non-inoculated samples in test 1-1, ×100

state evolution can be measured by analysing the thermal parameters and a structural relationship based on these parameters is possible.

According to the eutectoid transformation parameters shown in Table 3, the variation of ferrite amount produces significant changes in the solid state cooling curves corresponding to the inoculated experiments. In these samples, cooling rates and nucleation potentials are very similar, so the isolated influence of chemical composition can be clearly studied.

When ferrite content decreases (so that pearlite increases), solid state transformations occur at lower temperatures (Fig. 9*a*) and eutectoid recalescence clearly

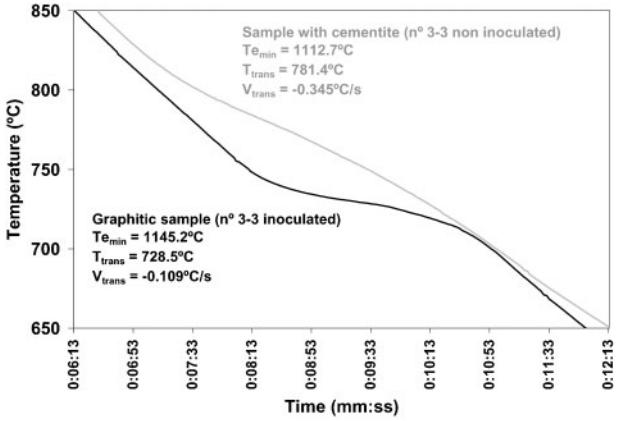

8 Comparison of eutectoid transition in white and graphitic cast irons

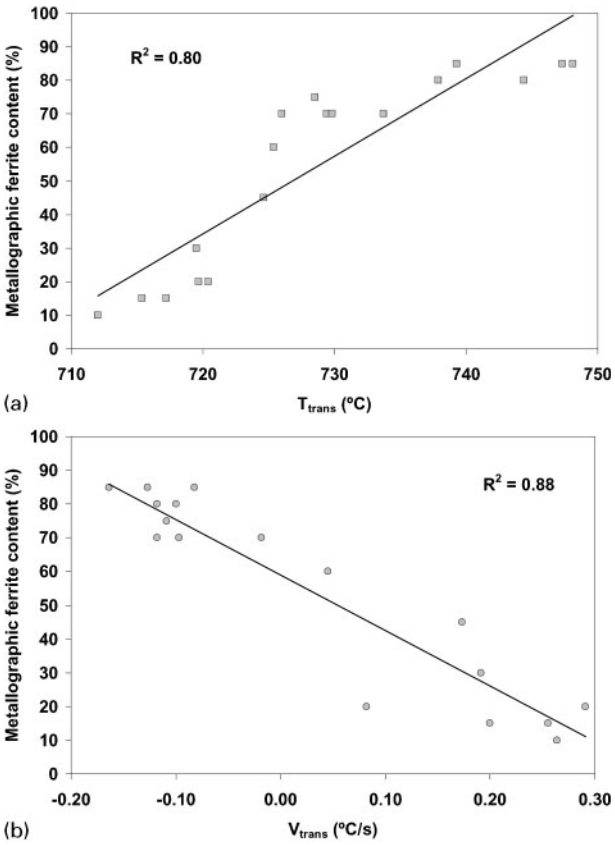

9 Structural evolution of *a* T_{trans} and *b* V_{trans} in eutectoid transformation of inoculated samples

increases. The last effect can also be considered by studying the evolution of the cooling rates in the middle of the eutectoid transformation V_{trans}. Gradual reductions in this thermal parameter are associated with larger pearlite amounts in inoculated nodular iron samples (Fig. 9*b*).

Eutectoid cementite formation (lamellar pearlite) provides bigger latent heat in comparison with only ferritic crystallisation.[17] Under these conditions, the solid state transitions are gradually more exothermic, recalescence appears and more positive values of V_{trans} are obtained.

In non-inoculated samples, a greater variability in the thermal curves is observed. This fact is due to the different nucleation potentials of the metal. So the last parameter plays a role just as important as the chemical composition. Under these conditions, the amount of graphitic nuclei decreases and carbon diffusion ability is reduced in solid austenite. Thus, the structural pearlite crystallisation is more possible in eutectoid range. According to these results, the final metallic structure can be expressed as

$$\text{Ferrite}(\%) = A_1 Te_{\min} + A_2 R + A3 I_G + A_4 Ve_{\max} + A_5 V_{trans} + A_6 \quad (1)$$

where $Te_{\min}$ is the minimum eutectic temperature, R is the eutectic recalescence and V_{trans} is the cooling rate at the centre of solid state transition (Fig. 5). $Ve_{\max}$ is the maximum cooling rate at the final step of eutectic transformation ($T_{solidus}$ zone) and I_G is the graphite growth factor at eutectic range. The last parameter was calculated from eutectic curves[16] according to the

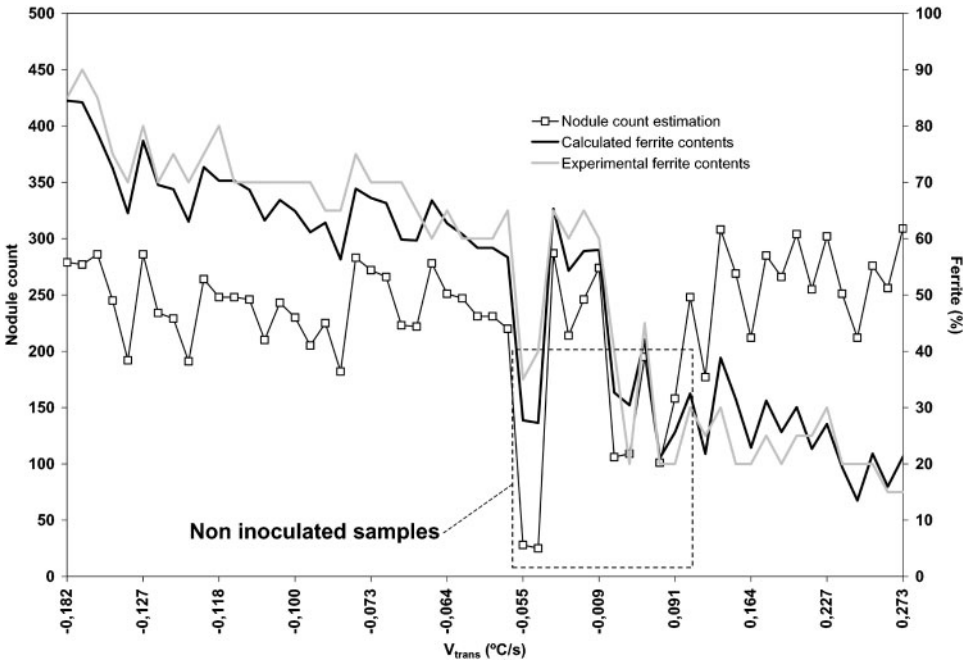

10 Comparison of experimental and calculated values of ferrite contents

following expression

$$I_G = \frac{M_g}{t_g} = \frac{M_{sample}\left[\%C_{sample} - \left(2{\cdot}03 - 0{\cdot}20 \times \%Si_{sample}\right)\right]}{100 t_g} \quad (2)$$

where t_g represents the graphite growth time in the eutectic range. This parameter is obtained from the comparison of the temperature evolution between the solidification of the sample (transformation area) and the cooling process of a theoretical sample without transformation.

When eutectic cementie is detected by the thermal cooling curves, the austenite formation process and transformation energies obtained greatly change with respect to the iron–graphite solidification pattern and equation (1) is not applicable.

In order to evaluate the predictive model developed in the present work, a comparison study of ferrite contents estimated using equation (1) and those obtained by metallographic inspections is presented (Fig. 10). Thus, a group of 56 inoculated and non-inoculated nodular iron samples were thermally analysed and their structural ferrite was compared. Different chemical compositions of iron are used to obtain more representative results.

When the data presented in Fig. 10 are analysed, it is noticed that a good agreement between experimental and calculated ferrite contents occurs. As expected, the progressive reduction of cooling rate V_{trans} increases the ferrite amounts in the analysed samples. In most cases the estimated nucleation potentials, expressed as nodules/mm^2, are located in the range of 200–300 (inoculated samples).

However, lower nodule densities (<120 nodules mm^{-2} at non-inoculated samples) can strongly increase the pearlite contents for similar V_{trans} values, according to the experimental model developed in the present work. In these cases, calculated ferrite estimations represent the real structure observed via metallographic inspections.

The structural tendency estimation obtained on these nodular iron samples does not include the influence of different cooling rates of real castings. This thermal parameter also plays an important role in the solid state transformation and can be considered in terms of geometric modulus. These studies will be the subject of future work.

Conclusions

The solidification and subsequent solid state transformation of SG iron were investigated using different chemical compositions and nucleation potentials. Both parameters can be measured and later evaluated by means of the cooling curves recorded in the range of 1210–600°C.

An experimental correlation between the thermal results and the final structure of iron can be detected taking into account the different nucleation potentials of iron at the pouring devices in addition to further inoculation treatments. The evidence presented in the present paper showed that the solid state structure mainly depends on chemical composition as much as the nucleation ability of iron during its solidification process. In ordinary conditions, inoculated SG iron provides similar nucleation potentials and critical element contents (Cu, Mn for instance) become the most important aspect.

These parameters in combination with the cooling rate of iron lead to the crystallisation of austenite and modify the carbon diffusion process from austenite or liquid iron to graphite centres, so different room temperature structures are obtained. Thermal analysis experiments made on standard iron samples (similar cooling rates) indicate that curve characteristics can estimate the final structure (ferritic, pearlitic and/or cementite type).

Using metallographic inspections on these standard samples makes it possible to confirm these features and

to establish a mathematical model in order to predict the ferrite/pearlite contents in thermally analysed SG iron samples. Thus, the structural tendency of iron can be evaluated before pouring and an important preventive tool is developed in order to ensure the production of castings with the desired final properties.

Acknowledgements

The present work forms part of a general research programme for thermal analysis techniques application in casting processes, managed by Azterlan Foundry Centre. The authors would like to thank Professor Doru M. Stefanescu for revising the present paper and Betsaide, S.A.L. for financial support.

References

1. R. W. Heine: *AFS Trans.*, 1995, **103**, 199–206.
2. R. W. Heine: *AFS Trans.*, 1986, **94**, 391–402.
3. C. Labrecque and M. Gagné: *AFS Trans.*, 1998, **106**, 83–90.
4. I. G. Chen and D. M. Stefanescu: *AFS Trans.*, 1984, **92**, 947–964.
5. U. Ekpoom and R. W. Heine: *AFS Trans.*, 1981, **89**, 27–38.
6. J. Tinoco, P. Delvasto, O. Quintero and H. Fredriksson: *Int. J. Cast Met. Res.*, 2003, **16**, 53–58.
7. D. M. Stefanescu: *MRS Symp.*, 1985, **34**, 151–162.
8. P. Zhu and R. W. Smith: *AFS Trans.*, 1995, **103**, 601–609.
9. F. J. Bradley and C. A. Fung: *Can. Metall. Q.*, 1991, **30**, (4), 251–260.
10. G. R. Strong: *AFS Trans.*, 1983, **91**, 151–156.
11. A. Louvo, E. Pellikka, J. Alhainen and P. Eklund: *AFS Trans.*, 1991, **99**, 237–244.
12. J. Lacaze: Proc. 4th Congreso Internacional de Materiales, Saltillo, Mexico, October 1997, Universidad de Saltillo, 1–12.
13. X. Guo and D. M. Stefanescu: *AFS Trans.*, 1997, **105**, 533–544.
14. E. F. Ryntz, Jr: *AFS Trans.*, 1976, **82**, 551–554.
15. AFS: 'Reference microstructure for measurement of pearlite and ferrite content in ductile iron microstructures', AFS current information report, Quality Control Committee 12-E, Ductile Iron Division, 1984.
16. R. Suárez: Proc. 1st Symp., Bilbao, Spain, July 2002, Azterlan and the Foundry Sector.
17. D. J. Celentano: *Int. J. Plast.*, 2001, **17**, 1623–1658.